Fuel 198 (2017) 31–41

Contents lists available at ScienceDirect

Fuel

journal homepage: www.elsevier.com/locate/fuel

Full Length Article

W and Mo doped TiO_2: Synthesis, characterization and photocatalytic activity

Osmín Avilés-García [a], Jaime Espino-Valencia [a,*], Rubí Romero [b], José Luis Rico-Cerda [a], Manuel Arroyo-Albiter [a], Reyna Natividad [b,*]

[a] Facultad de Ingeniería Química, Universidad Michoacana de San Nicolás de Hidalgo, Edif. V1, Ciudad Universitaria, 58060 Morelia, Michoacán, Mexico
[b] Chemical Engineering Lab., Centro Conjunto de Investigación en Química Sustentable, UAEMéx-UNAM, Universidad Autonoma del Estado de Mexico, km 14.5 Toluca-Atlacomulco Road, San Cayetano, Toluca, Estado de México, Mexico

HIGHLIGHTS

- Doping of TiO_2 with W or Mo leads to a higher photo-activity.
- Low content of W or Mo is related to the best performance of TiO_2 as photocatalyst.
- Addition of dopants eliminates the need of oxygen addition.

GRAPHICAL ABSTRACT

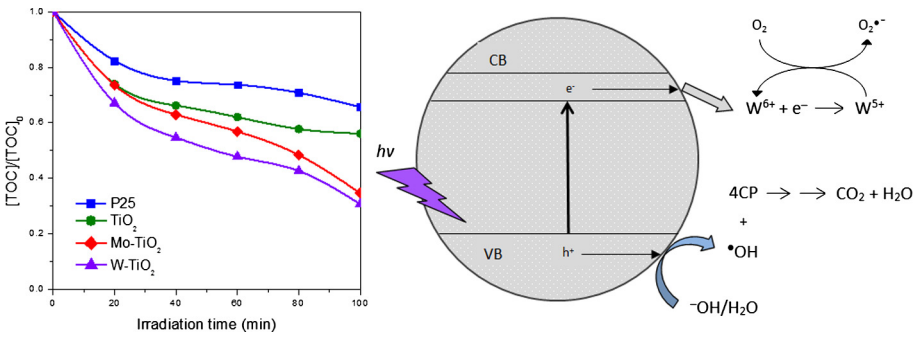

ARTICLE INFO

Article history:
Received 15 May 2016
Received in revised form 29 August 2016
Accepted 2 October 2016
Available online 17 October 2016

Keywords:
Doped TiO_2
Tungsten
Molybdenum
Electron traps
Photocatalysis

ABSTRACT

W-doped TiO_2 and Mo-doped TiO_2 photocatalysts were synthesized by EISA method and were characterized by different techniques. The photoactivity of these materials was evaluated by the degradation of 4-chlorophenol without oxygen supply. The catalysts exhibited only anatase crystalline phase and high specific surface areas of about 179 $m^2\ g^{-1}$. The amount of dopant cations in TiO_2 was a key parameter to increase the photoactivity. The results obtained show that with low dopant concentrations the degradation is improved, and this can be attributed to an increase in the lifetime of the photogenerated charges due to that dopant cations may easily trap electrons decreasing the recombination rate. Doped photocatalysts degraded 95% of 4CP, three times faster than Degussa P25. 69% reduction of total organic carbon (TOC) content was achieved by 1 wt.% W-doping.

1. Introduction

The degradation and mineralization of organic pollutants in water and air by photocatalysis with TiO_2 has been addressed by many researches [1,2]. The photocatalytic activity of titania is highly dependent on its crystal structure and on its ability to generate hole (h^+)/electron (e^-) pairs on the catalytic surface. In addition, TiO_2 in its anatase crystalline phase is activated only with ultraviolet (UV) light with a band-gap energy of 3.2 eV. Therefore, modification of titania by doping with transition metals has been of great interest to improve its photocatalytic activity and extend its light absorption capacity towards the visible light region [3]. While this is true, the decrease in recombination rate between excited hole/electron pairs should not be completely left aside. The objective of this work is to present the effect of the incorporation of transition metals tungsten (W) or molybdenum (Mo) on the photoactivity of nanocrystalline anatase TiO_2.

* Corresponding authors.
E-mail addresses: jespinova@yahoo.com.mx (J. Espino-Valencia), reynanr@gmail.com (R. Natividad).

http://dx.doi.org/10.1016/j.fuel.2016.10.005
0016-2361/

The method used for the synthesis of the materials is known as Evaporation Induced Self Assembly (EISA). This method has been employed for the preparation of mesostructured metal oxides by using surfactants allowing the formation of an organized liquid-crystal together with an inorganic condensation [4]. Moreover, it has been observed that mesoporous titania synthesized by the EISA methodology has positive effects on degradation, since it is possible to obtain unique structures and properties such as unimodal pore size distributions and high surface areas [5]. The synthesized photocatalysts were tested in the photocatalytic degradation of 4-chlorophenol.

Chlorophenols (CPs) are a class of compounds widely used considered as priority pollutants due to its recalcitrance, toxicity as well as potentially mutagenic and carcinogenic to both aquatic and terrestrial life according to the United States Environmental Protection Agency [6]. The presence of CPs in the wastewater can be attributed to different origins in the manufacture of solvents, herbicides, dyestuffs, pesticides, paper, petrochemicals and pharmaceuticals. Among CPs, the photocatalytic degradation of 4-chlorophenol (4CP) with TiO_2 has been the subject of many investigations [7,8] because it is taken as a model molecule to evaluate the photoactivity of catalysts which is representative of chlorinated phenolic pollutants [9,10]. The incorporation of cations as dopants within the crystal structure of TiO_2 to enhance photocatalytic activity by intervening in the photogenerated charges during degradation of 4CP under UV and visible light irradiation, as well as the identification of intermediate compounds has also been studied [11,12]. Although there are a lot of investigations related to the activation of titanium dioxide using visible light radiation, it remains unclear the effect of doping to inhibit recombination of electron/-hole pairs during the photocatalytic activity. For this reason, we evaluated the effect of titania doped with W or Mo not only in the 4CP degradation/mineralization but also in the properties of the photogenerated charges.

2. Experimental

2.1. Materials

All chemicals used for the synthesis of the catalysts were of analytical grade. Titanium (IV) butoxide [$Ti(OC_4H_9)_4$, 97% Sigma-Aldrich) was used as precursor of titanium species. Ammonium molybdate tetrahydrate [$(NH_4)_6Mo_7O_{24}{\cdot}4H_2O$, Aldrich] and ammonium metatungstate hydrate [$(NH_4)_6H_2W_{12}O_{40}{\cdot}xH_2O$, Aldrich] were used as the sources for Mo and W respectively. P123 triblock copolymer [poly(ethylene glycol)-block-poly(propylene glycol)-block-poly(ethylene glycol), $EO_{20}PO_{70}EO_{20}$, Sigma-Aldrich] was used as the structure directing agent (SDA). Nitric acid (HNO_3, 70%, Aldrich) was employed as catalyst and ethyl alcohol (C_2H_6O, 99.5%, Aldrich) was used as solvent. 4-chlorophenol (ClC_6H_4OH, 99%, Aldrich) was used as the model contaminant to study the photo-activity of the synthesized materials.

2.2. Preparation of TiO_2, W-TiO_2 and Mo-TiO_2

The catalysts synthesis was carried out by EISA method using copolymer P123. To synthesize pure mesoporous TiO_2 the following molar ratio of reactants was used, 1 $Ti(OBu)_4$:18.71 ethanol:0.018 P123:3.55 HNO_3. The synthesis was conducted as follows: an alcoholic solution of $Ti(OBu)_4$ was prepared and then stirred for 15 min. This solution was incorporated to the SDA with vigorous stirring for 30 min and finally the HNO_3 was dropwise added with constant stirring to the reaction media. The obtained mixture was subsequently sealed and kept under stirring for 3 h at room temperature. After this time, the solution was transferred to a rotary evaporator (Heidolph precision ML/G3 model) for 17 h. The resulting solid material was first calcined at 300 °C for 1 h under slow heating rate of 1 °C min^{-1} to remove the SDA, and then at 400 °C to obtain a crystalline material with open pores. Doped TiO_2 materials were synthesized based on the aforementioned procedure by incorporating tungsten and molybdenum precursors (with 1 wt.%, 2 wt.% and 3 wt.% of doping to theoretical titania in nominal weight percentages) after adding the SDA, thereby obtaining W-TiO_2 and Mo-TiO_2 photocatalysts. Degussa P25 (commercial titania) was employed for comparative reasons as reference photocatalyst.

2.3. Characterization

The crystalline structure of all synthesized materials was determined by X-ray diffraction analysis by using a D8 Advance Bruker equipment with Cu Kα radiation at 0.15406 nm. A current of 25 mA and voltage of 30 kV were used. The diffractograms were scanned from 20° to 70° 2θ in steps of 0.02°/16 s. Scherrer equation ($D = k\lambda/S\cos\theta$) was applied to estimate the average crystallite size of the solid catalysts through the full width at half maximum of the anatase peak (1 0 1), while lattice distortions (ε) were obtained from $\varepsilon = S/4\,tg\,\theta$, where D is the crystal size, k is a coefficient that depends on crystallite form typically with a value of 0.9, λ is the applied radiation wavelength, S is the half-height width of the diffraction peak of anatase, and θ is the diffraction angle.

The adsorption–desorption isotherms by using liquid nitrogen (77 K) were obtained in an Autosorb-1 Quantachrome sorption equipment to determine the specific surface area and average pore diameter of all synthesized samples. The materials were first outgassed to eliminate the moisture at 200 °C for 2 h before adsorption measurements. The pore size distributions and the specific surface areas of the catalysts were estimated by BJH (Barrett–Joyner–Halenda) and BET (Brunauer–Emmett–Teller) methodologies, respectively.

UV–vis absorption spectra by diffuse reflectance of the photocatalysts were obtained using a Labsphere RSAPE-20 integration sphere within a Lambda 35 Perkin Elmer spectrometer. The band gaps of the as synthesized materials were estimated by the Kubelka–Munk function.

The crystalline particle size and morphological properties of the samples were examined by SEM (scanning electron microscopy) using a JEOL JSM-6510LV model with an accelerating voltage of 20 kV, and TEM (transmission electron microscopy) in a JEOL-2100 model working at 200 kV equipped with a LaB6 filament.

To determine the oxidation states of the chemical elements on the surface of the synthesized materials, XPS (X-ray photoelectron spectroscopy) was carried out in a JEOL JPS-9200 spectrometer by using Al Kα as X-ray radiation source. All the binding energies determined were referenced to energy of 284.6 eV corresponding to the C 1s peak.

2.4. Photocatalytic activity studies

The heterogeneous photocatalytic oxidation of 4-Chlorophenol (4CP) was carried out in a batch reactor with capacity of 70 ml as total reaction volume. The initial concentration of 4CP was 0.156 mmol L^{-1}. The temperature inside the reactor was maintained constant at 25 °C during reactions. The initial pH of the 4CP solution was adjusted to a value of 2 with a 3 M HCl solution. The radiation source was a UV lamp with emission wavelength of 254 nm and intensity of about 4500 μW cm^{-2}. The lamp was dipped at the center of the reactor in order to completely irradiate the 4CP solution. The catalyst loading was 0.2 g L^{-1} and stirring was kept constant at 1000 rpm. Every 20 min aliquots were taken

of the suspension and then centrifuged at 13,000 rpm for 10 min to remove the catalyst prior analysis.

The concentration of 4CP with respect to the reaction time was analyzed by measuring the absorbance at 280 nm corresponding to the absorption peak of 4CP. Measurements were determined with a Lambda 25 UV–vis spectrophotometer (Perkin-Elmer) between 200 and 360 nm. A calibration curve (from 0 to 0.233 mmol L^{-1}) was generated to calculate the actual concentration, obtaining a correlation coefficient (r^2) equal to 0.9998 and a slope of $\varepsilon b = 0.0116$ based on the Beer-Lambert law.

The mineralization of 4CP was determined by using equipment that allows the quantification of total organic carbon (TOC-L, Shimadzu). The solutions were immediately analyzed after being centrifuged.

3. Results and discussion

3.1. Catalysts characterization

3.1.1. N_2 adsorption-desorption and XRD analysis

The diffraction patterns of undoped and doped titania with tungsten (W) or molybdenum (Mo) cations are presented in Fig. 1. All samples exhibited reflections attributed only to the anatase crystalline phase at 2θ: 25, 38, 48, 54, 55 and 63 approximately, which correspond to the (1 0 1), (0 0 4), (2 0 0), (1 0 5), (2 1 1) and (2 0 4) planes [13]. The intensity of (1 0 1) diffraction peak decreases for some doped samples in comparison to the pure TiO_2 sample. This implies that the doping could curb the phase transition and inhibit the crystalline growth as shown in Table 1. This is clearly observed for W-doped TiO_2 samples (Fig. 1a). A careful observation of (1 0 1) peak (Fig. 1b and d) leads to detect a slight shift to lower 2θ grades with respect to TiO_2 sample, which is a consequence of the incorporation of W and Mo ions in the TiO_2 lattice. In numerical terms, the ionic radius of Ti^{4+} (0.0605 nm) [14] is very close to the ionic radii of W^{6+} (0.060 nm) [15] and Mo^{6+} (0.062 nm) [16], so that these can take the place of titanium inside crystal lattice [17]. In addition, the increase in the distortion of the crystal lattice is another characteristic due to doping, which can be confirmed by the results in Table 1. The DW3 and TiO_2 samples exhibited crystal sizes of 6.1 nm and 8.6 nm respectively, but DW3 presented 28% higher lattice distortion than TiO_2. Therefore, it a low crystallinity is related with greater distortion caused with increasing doping.

The textural properties of samples according to synthesis method are shown in Table 2. It can be observed that by incorporating dopant cations in the mesoporous titania the specific surface area is increased with respect to undoped titania [18], which exhibited specific surface area of 144 $m^2 g^{-1}$. Mo-doped TiO_2 materials showed specific surface areas of around 163 $m^2 g^{-1}$. The increase in weight percentage of Mo increased the specific surface

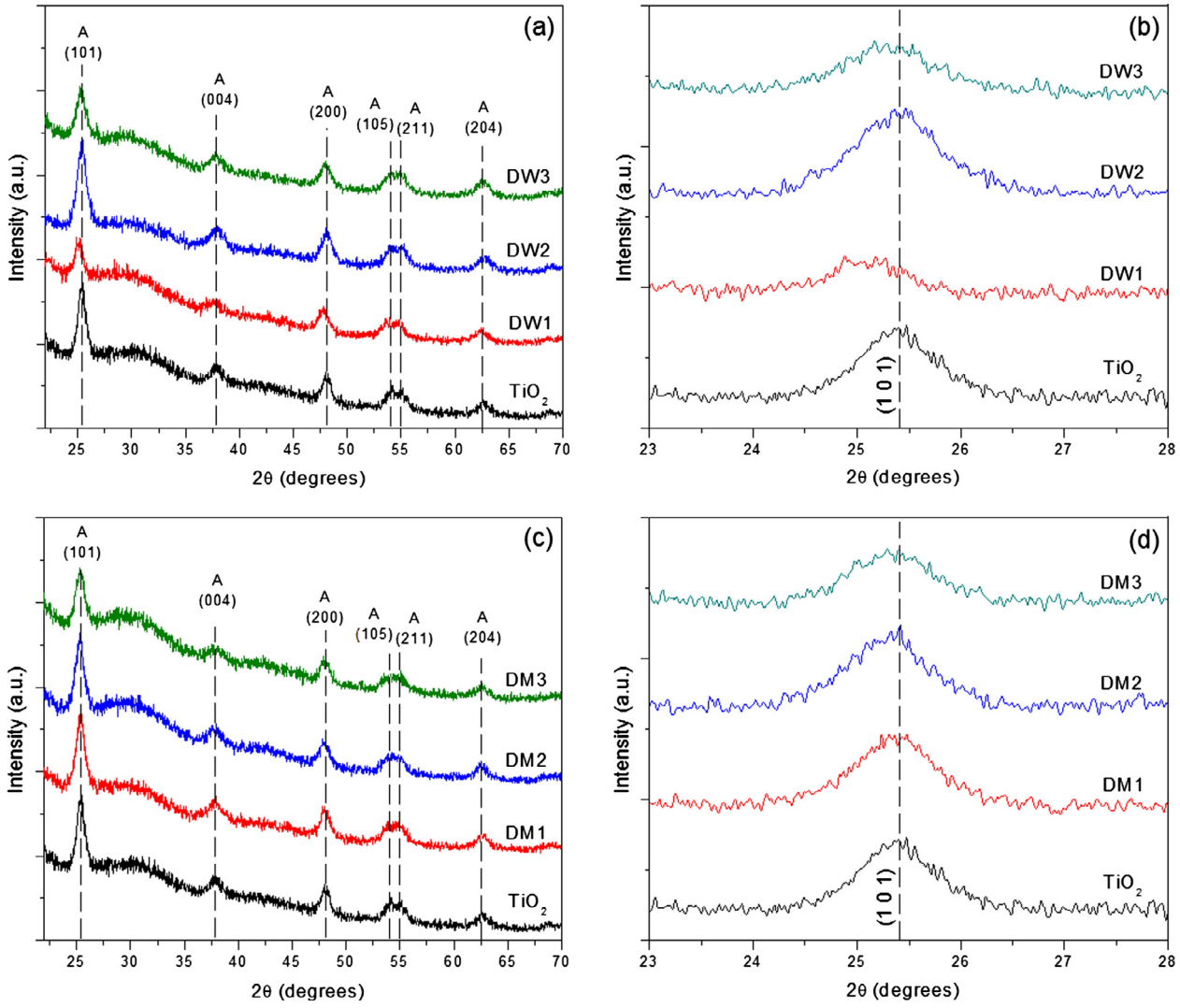

Fig. 1. (a and c) XRD patterns (b and d) diffraction profiles on (1 0 1) plane of W-doped TiO_2, Mo-doped TiO_2 and undoped TiO_2 samples.

Table 1
Crystallite parameters of undoped and doped titania with W or Mo cations.

Sample ID	wt.% W	wt.% Mo	Average crystallite size (nm)	(1 0 1) interplanar distance (nm)	Lattice distortion ε
TiO_2	0	0	8.6	0.3495	0.0183
DW1	1	0	7.4	0.3577	0.0217
DW2	2	0	8.1	0.3511	0.0195
DW3	3	0	6.1	0.3486	0.0255
DM1	0	1	8.1	0.3527	0.0196
DM2	0	2	8.6	0.3504	0.0183
DM3	0	3	7.7	0.3519	0.0205

Table 2
Specific surface area and average pore size of undoped and doped TiO_2 with W or Mo cations.

Sample ID	Specific surface area ($m^2\ g^{-1}$)	Average pore size (nm)
TiO_2	144	6.1
DW1	151	6.1
DW2	160	4.6
DW3	179	4.6
DM1	151	6.1
DM2	161	6.1
DM3	163	6.1

area albeit the average pore diameter at a value of 6.1 nm remains constant. W-doped TiO_2 samples exhibited specific surface areas of approximately 179 $m^2\ g^{-1}$. In the same way, an increase in specific surface area by increasing the loading of W was observed, but in this case the average pore diameter decreased from 6.1 to 4.6 nm when the amount of W increased from 1 to 2 wt.%. This trend suggests that an increase in dopant content into TiO_2 structure could increase the specific surface area and reduce the average pore diameter because crystal growth is confined [19], which is confirmed by XRD results (see Table 1).

Fig. 2 shows the N_2 adsorption–desorption isotherms and pore size distributions of synthesized samples. All these materials

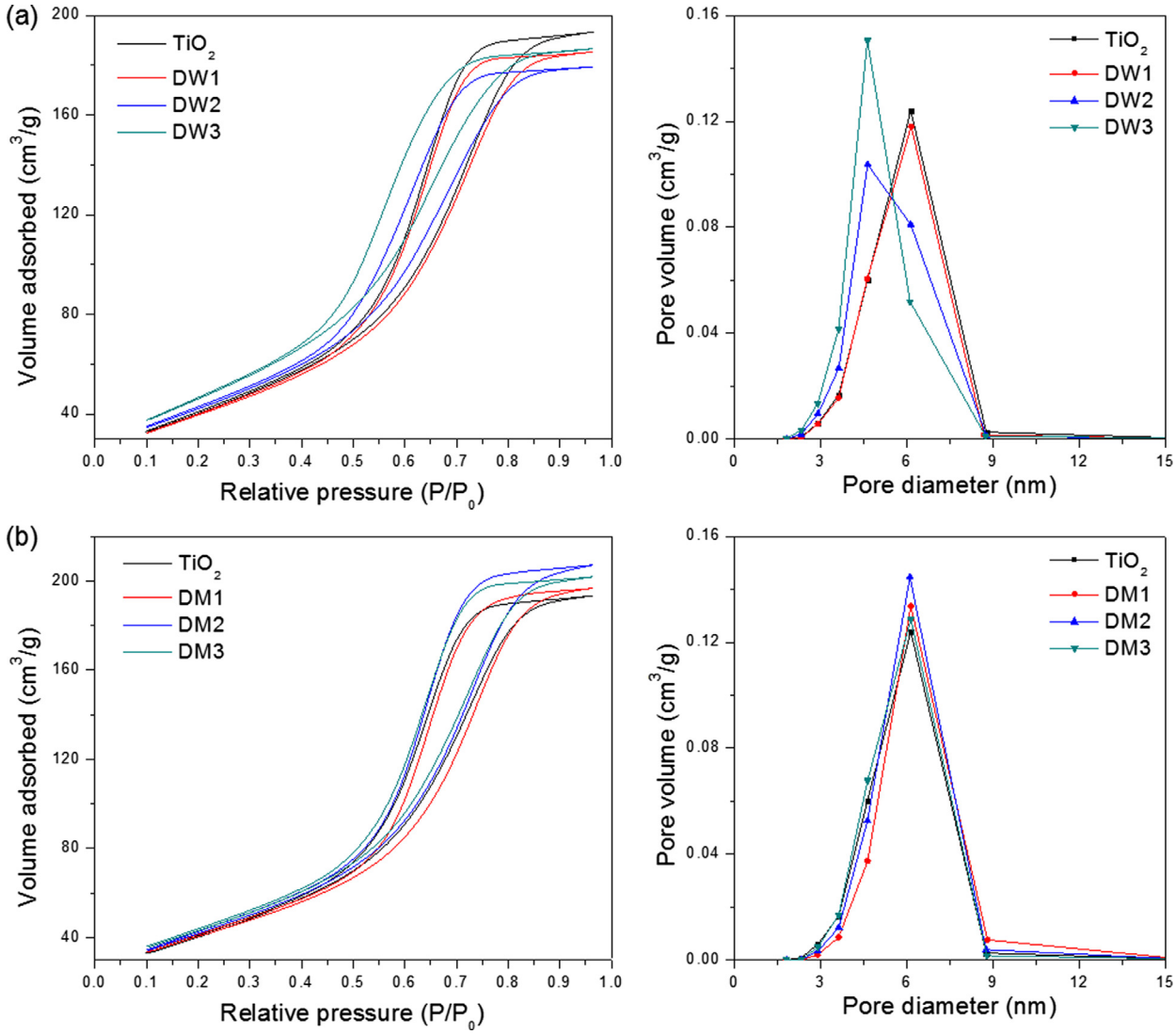

Fig. 2. N_2 adsorption-desorption isotherms and pore size distribution of (a) W-doped TiO_2 and (b) Mo-doped TiO_2 and undoped TiO_2.

presented type IV isotherms with hysteresis loops, which confirm the mesoporosity of the catalysts. Also, the presence of non-uniform pores forming large channels is due to type H2 hysteresis situated between 0.5 and 0.9 of relative pressure [20].

The reference TiO_2 (P25) consists of rutile and anatase crystalline phases with crystallite size of 32 nm and specific surface area of 50 $m^2 g^{-1}$ [21].

3.1.2. TEM and SEM analysis

The microstructures with the highest photoactivity (DW1 and DM1 samples) and TiO_2 sample were analyzed by TEM (transmission electron microscopy) and HRTEM (high resolution transmission electron microscopy) techniques. Fig. 3 shows the TEM images with their SAED (selected area electron diffraction) patterns (inset) and HRTEM images of samples, respectively. It can be clearly seen that the materials are formed by small crystals of about 7–9 nm in size. This in concordance with the results determined by Scherrer equation in the XRD analysis. In addition, the SAED in the inset of Fig. 3 shows a sequence of Debye rings consistent with crystalline planes of anatase phase. The undoped sample exhibited more defined rings because the doping with W or Mo ions delays the crystalline phase transition [22]. The distance between the parallel fringes (see Fig. 3) was determined to be of approximately 0.35 nm, which is assigned to the preferential crystalline growth direction for (1 0 1) plane of TiO_2 anatase.

The SEM images of undoped and doped titania are shown in Fig. 4. The doped samples exhibited particles with irregular morphology and sizes from 50 to 80 μm (Fig. 4a and b) while the undoped sample presented smaller and less uniform particles of about 20–80 μm (Fig. 4c). The reference catalyst (Degussa P25) is a material composed of anatase and rutile crystalline phases forming elementary particles of 85 and 25 nm, respectively [23].

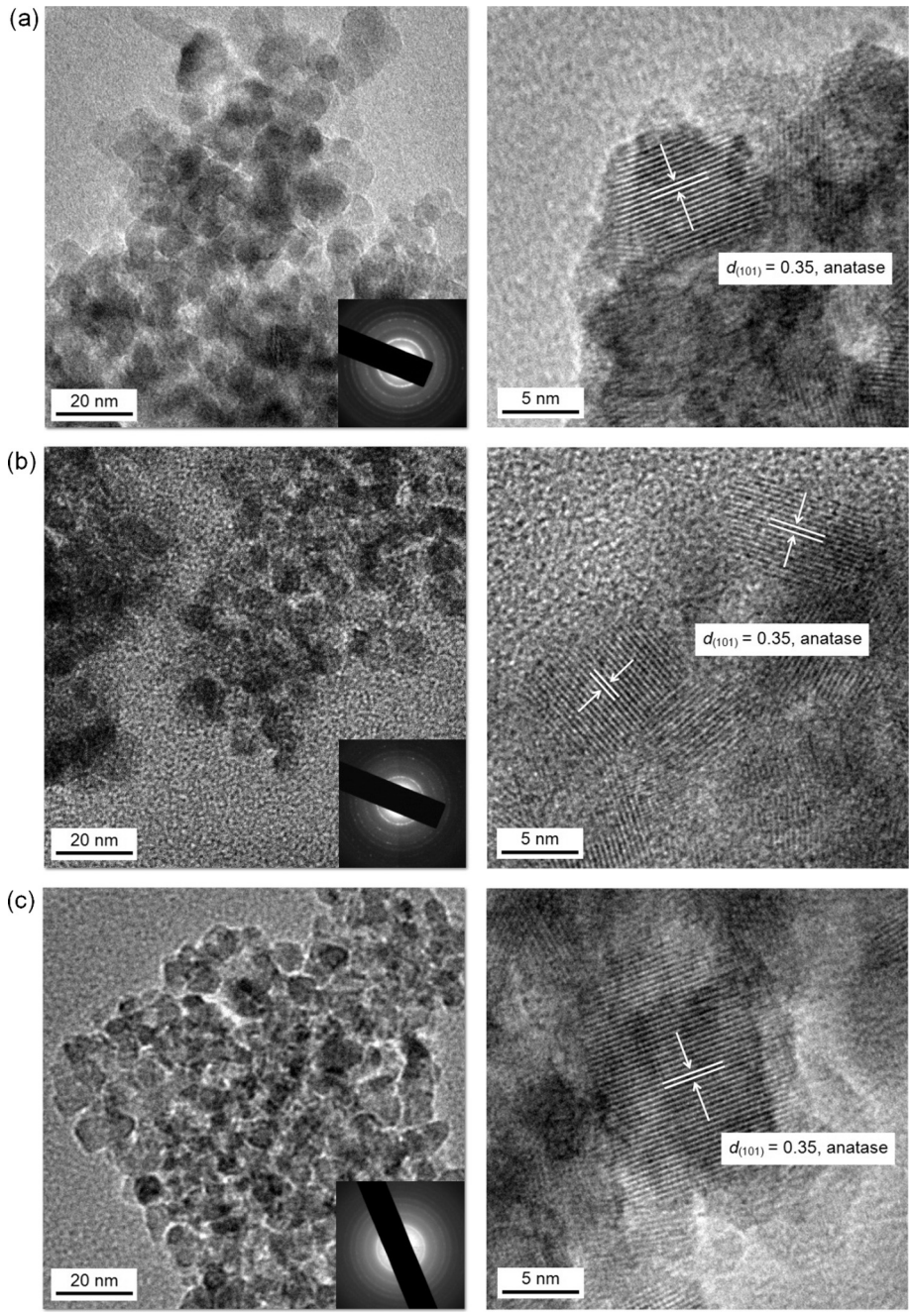

Fig. 3. TEM images, SAED patterns (inset) and HRTEM images of (a) DW1, (b) DM1, and (c) TiO_2 samples.

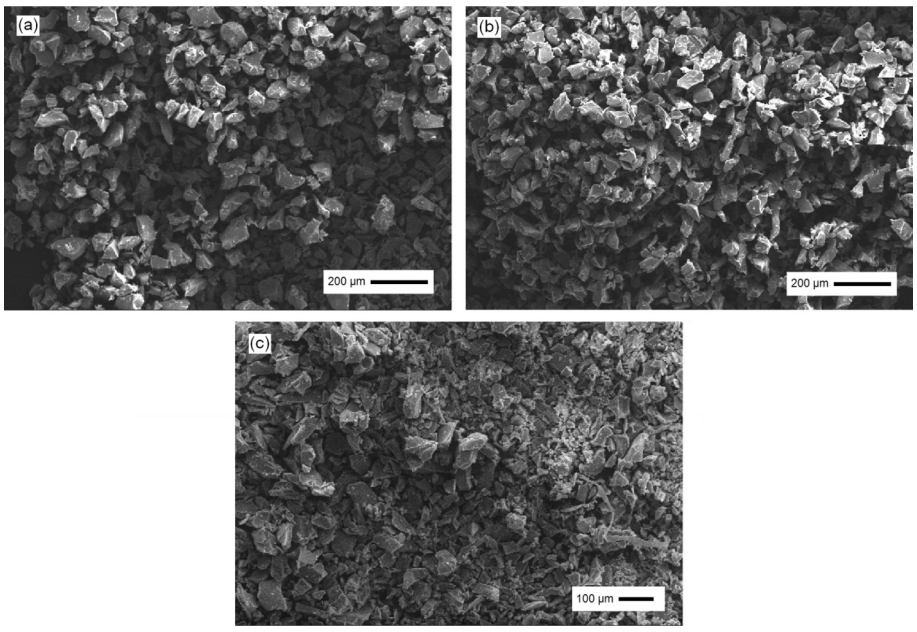

Fig. 4. SEM images of (a) DW1, (b) DM1, and (c) TiO_2 samples.

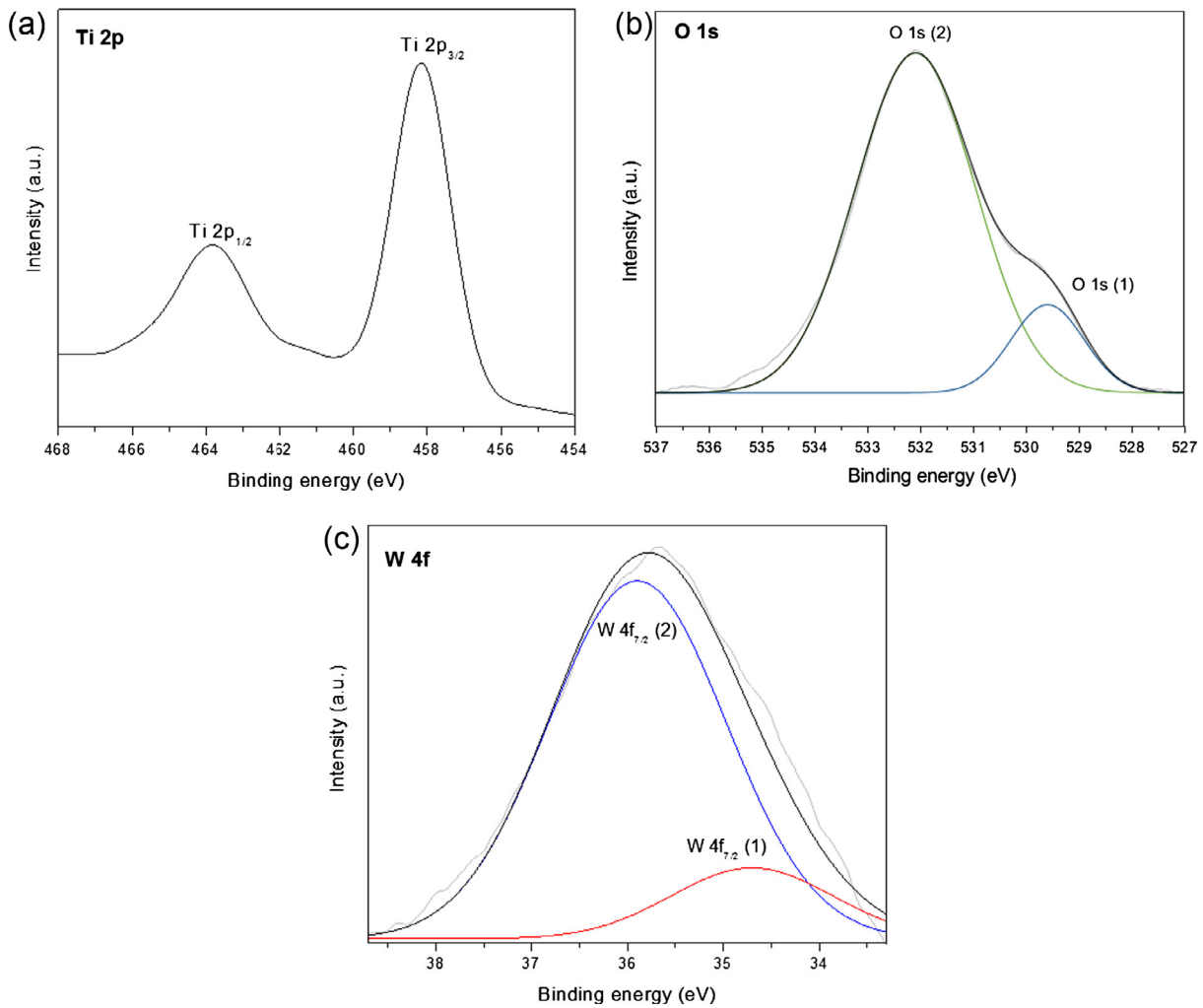

Fig. 5. XPS spectra of (a) Ti 2p, (b) O 1s, and (c) W 4f of the sample DW1.

3.1.3. XPS and DRS analysis

To determine the chemical states of the species on the surface of the W-doped TiO_2 and Mo-doped TiO_2 materials, XPS spectra were acquired and analyzed through the binding energies (BE) of W 4f, Mo 3d, Ti 2p and O 1s. The electronic states Ti 2p1/2 and Ti 2p3/2 correspond to two peaks with binding energy of 463.8 eV and 458.1 eV, respectively (see Figs. 5a and 6a), and this confirms the presence of Ti^{4+} species in TiO_2 lattice [24]. Fig. 5c shows the XPS spectra in the W 4f region of the sample DW1. As seen from this figure, two components at about 35.9 eV and 34.7 eV correspond to W 4f7/2 state in the forms W^{6+} and W^{5+} (see Table S1) [25]. The ratio of peak areas is 5.5:1.0, so that the percentage of W^{6+} is 84.7% and W^{5+} is 15.3%, this means that few ions are present as W^{5+} species. Fig. 6c shows the XPS spectra of the sample DM1. Mo 3d spectrum exhibits a double peak at 232.2 eV and 235.3 eV, which correspond to Mo 3d5/2 and Mo 3d3/2 states of Mo^{+6} cations [26]. The other peaks with binding energies of 231.3 eV and 234.3 eV are characteristic of species Mo^{5+} (see Table S2) [27]. The percentage of Mo^{6+} and Mo^{5+} ions is 75.3% and 24.7%, respectively. Therefore, the incorporation of W and Mo ions within TiO_2 lattice coexist in DW1 and DM1 samples as W^{6+}/W^{5+} and Mo^{6+}/Mo^{5+}. On the other hand, the presence of W^{5+} and Mo^{5+} ions in the synthesized samples implies the existence of oxygen vacancies due to the incorporation of dopant cations. In Figs. 5b and 6b, the XPS spectra of O 1s electronic state are presented. This spectrum is formed by the contribution of two peaks, the first at 529.6 eV attributed to O^{2-} within lattice TiO_2 [28], and the second at 532.1 eV can be assigned to surface hydroxyl groups. The hydroxyl groups are beneficial for oxidation reactions, because they act as adsorption sites of organic compounds and traps of photogenerated holes producing hydroxyl radicals, which directly attack the organic matter during the reactions of photodegradation [29].

All synthesized samples were analyzed by UV–vis diffuse reflectance spectroscopy (DRS) to estimate band-gap energies using the Kubelka-Munk function in order to obtain the absorption coefficient (α) through the diffuse reflectance,

$$\alpha \approx (1 - Re_\infty)^2 / 2Re_\infty = A/S \quad (1)$$

where Re_∞ is reflectance equal to $R_{sample}/R_{reference}$ for infinitely thick samples, S is scattering coefficient and A is absorption coefficient [30]. The value of $(\alpha h\nu)^2$ extrapolated to 0 corresponds to the band-gap energy (see Figs. 7 and 8). Fig. 7 shows the diffuse reflectance spectra of W-TiO_2 and TiO_2 samples. Undoped TiO_2 sample exhibited a band gap value of 3.23 eV, which concurs with the value reported in literature for pure anatase (3.20 eV) [31]. Doping of titania with tungsten ions did not significantly modify the TiO_2 absorption edge in the visible region (see Table S3). This may be because there are inside the conduction band of Ti 3d located the empty orbitals W 5d [32]. Fig. 8shows the diffuse reflectance spectra of

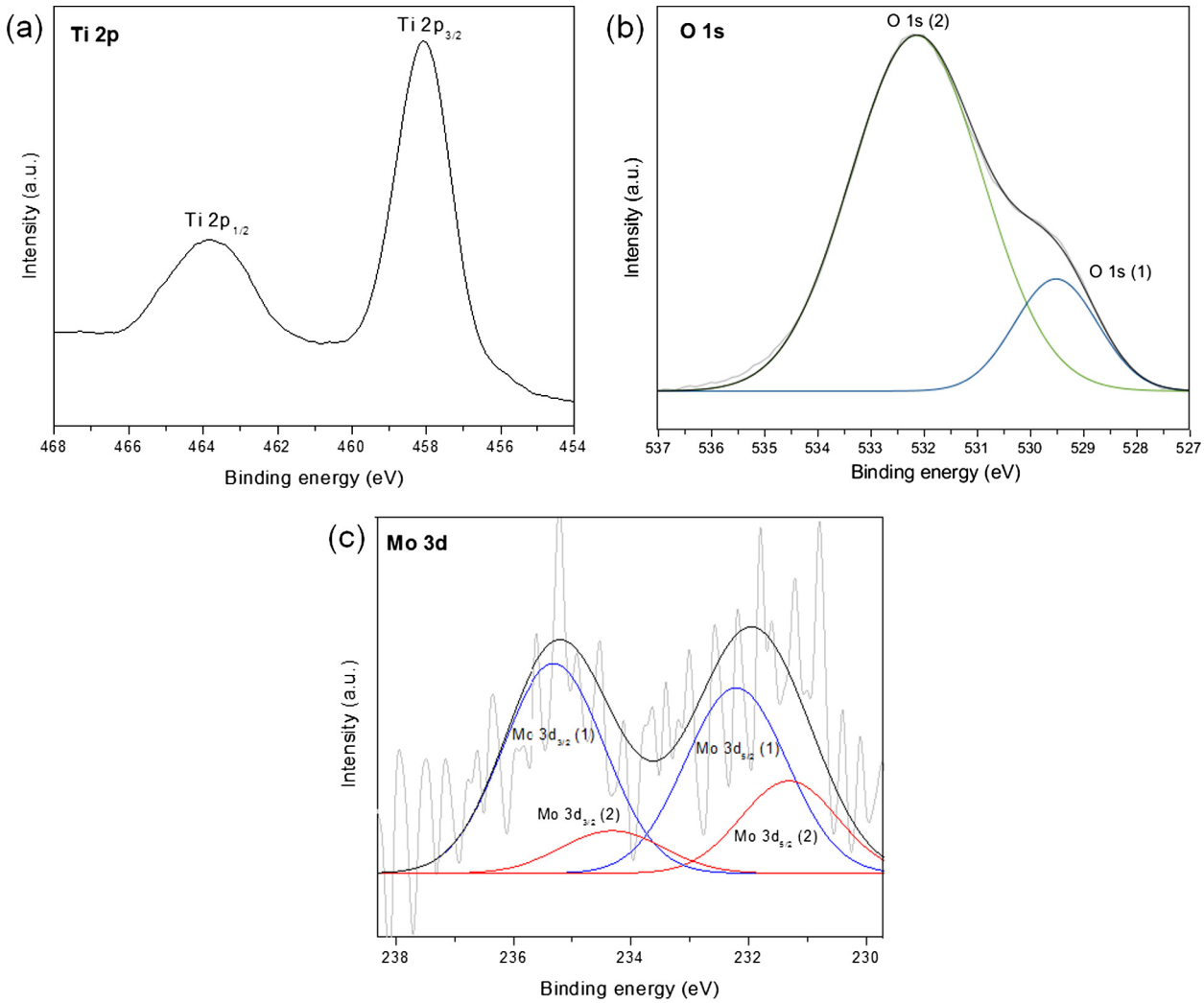

Fig. 6. XPS spectra of (a) Ti 2p, (b) O 1s, and (c) Mo 3d of the sample DM1.

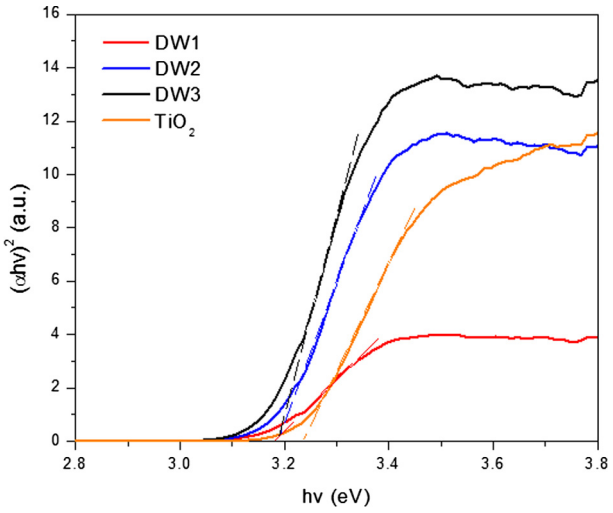

Fig. 7. Band-gap energy of undoped TiO_2 and W-doped TiO_2 samples.

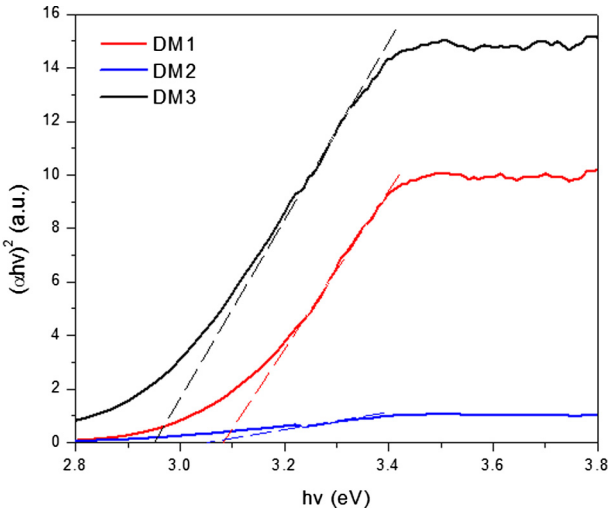

Fig. 8. Band-gap energy of Mo-doped TiO_2 samples.

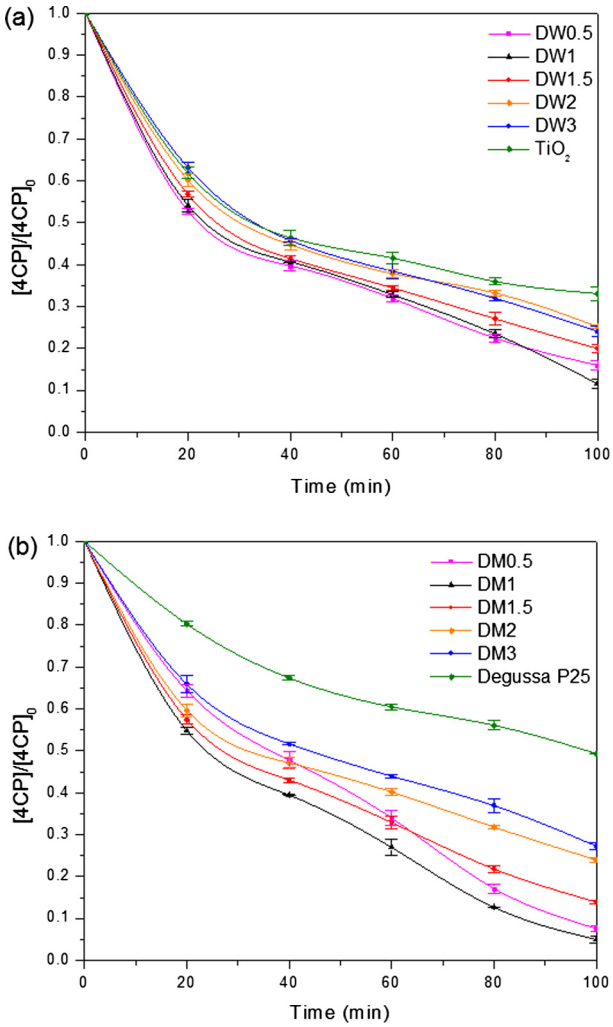

Fig. 9. Photocatalytic degradation profiles of 4CP over (a) W-doped TiO_2 and undoped TiO_2 samples (b) Mo-doped TiO_2 and Degussa P25 samples.

Mo-doped TiO_2 samples. These samples presented a clear red[1] shift of band gap compared to TiO_2 sample (see Table S3). By increasing the amount of Mo ions the band gap energy is decreased to a value of 2.95 eV (sample DM3). When transition metals n-type (Mo cations) are used as dopants for TiO_2, charge transfer transitions located at the bottom of the conduction band may occur due to interactions by band-gap states in titania and Mo orbitals 'd'. It is noteworthy that the used synthesis method, applied heat treatment and type of precursors are key parameters to obtain doped TiO_2 materials with absorption within visible region [33]. Moreover, W-TiO_2 and TiO_2 samples exhibited a very similar color, while Mo-TiO_2 samples present light gray color.

3.2. Photocatalytic activity

The photocatalytic activity of all synthesized materials was tested in the degradation of 4CP and Degussa P25 was used as reference material. Fig. 9 shows the photocatalytic degradation profiles of 4CP oxidation catalyzed with doped TiO_2, undoped titania and Degussa P25. All synthesized samples exhibited higher degradation percentage than Degussa P25 after 100 min of irradiation. A relationship between the percentage of degradation and the specific surface area of doped samples with different weight percentages of W or Mo cations was not observed. A relationship with the dopant content is observed though. Samples of TiO_2 doped with different amounts of W cation presented similar degradation profiles, but the sample doped with 1 wt.% showed the greatest degradation of approximately 88% as shown in Fig. 9a. The same trend for low dopant concentrations is observed in Mo-doped TiO_2 samples (see Fig. 9b). Sample DM1 with 1 wt.% Mo cation achieved 95% of 4CP degradation while sample DM3 with 3 wt.% degraded only 73% of 4CP. This concurs with previous related literature [34] and indicates that there is an optimum concentration for this type of dopant ions in the TiO_2 lattice. This has been suggested [35] to be due to an increased lifetime of photogenerated h^+/e^- pairs to carry out oxidation/reduction reactions on catalytic surface with adsorbed organic molecules. Under irradiation, the excited electrons are promoted to conduction band (Eq. (2)), which can be trapped by Mo^{6+} and W^{6+} ions reducing them to the species Mo^{5+} and W^{5+} (Eq. (3)). In this case, the photogenerated charges are efficiently trapped and the photocatalytic activity is improved since ions may be reduced [25,36], then electrons can be donated and trapped to and by oxygen molecules adsorbed on the surface of TiO_2 [37] or by benzoquinone (BQ) to form hydroquinone (HQ) (main formed species during 4CP degradation) [38], and finally ions can return to W^{6+} and Mo^{6+} (Eqs. (4) and (5)) (see Fig. 10).

[1] For interpretation of color in Fig. 8, the reader is referred to the web version of this article.

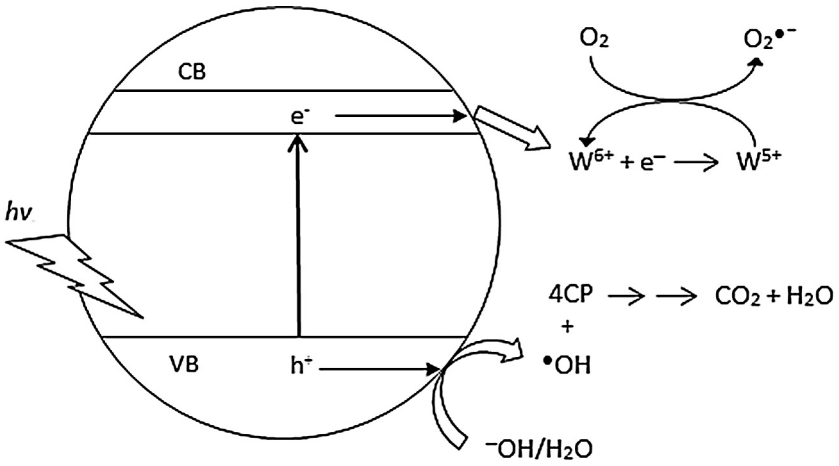

Fig. 10. Possible mechanism for degradation of 4CP in W-doped TiO_2.

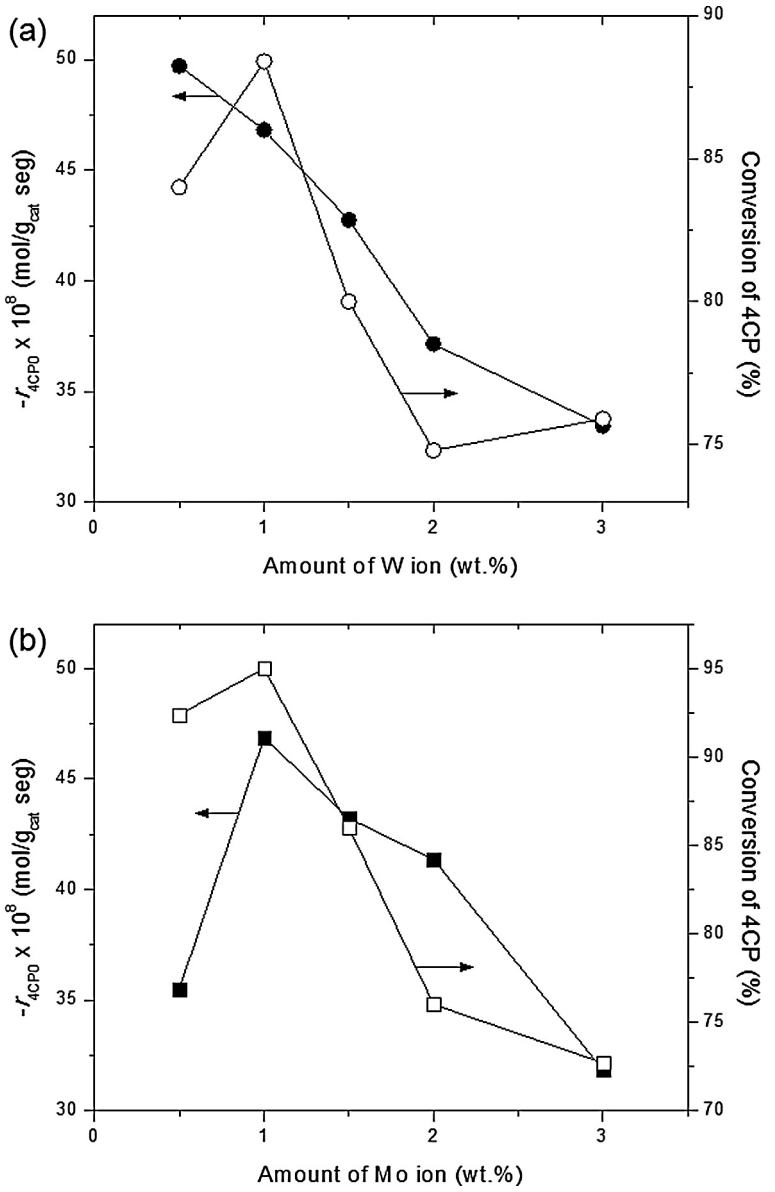

Fig. 11. Effect of the doping amount of (a) W ion and (b) Mo ion on the initial reaction rate and degradation percentage of 4CP. Reaction conditions: T = 298 K, Catalyst loading = 0.2 g L^{-1}, $t_{reaction}$ = 100 min.

$$W - TiO_2 + hv \rightarrow h^+_{vb} + e^-_{cb} \quad (2)$$

$$W^{6+} + e^-_{cb} \rightarrow W^{5+} \quad (3)$$

$$W^{5+} + O_2 \rightarrow W^{6+} + O_2^{\cdot -} \quad (4)$$

$$2W^{5+} + BQ + 2H^+ \rightarrow 2W^{6+} + HQ \quad (5)$$

The recombination rate of the generated charges is decreased during these processes by allowing the generation of a greater amount of hydroxyl radicals (·OH), which are responsible for the degradation of organic compounds (Eq. (11)) [39]. The ·OH radicals can be formed by two routes [7]: (i) photogenerated holes in the valence band reacting with the adsorbed water or with OH^- groups on the TiO_2 surface (Eqs. (6) and (7)) which is the main route of formation of hydroxyl radicals, (ii) via superoxide anion to form hydroperoxyl radical and hydrogen peroxide (Eqs. (8)–(10)).

$$h^+_{vb} + H_2O \rightarrow \cdot OH + H^+ \quad (6)$$

$$h^+_{vb} + OH^- \rightarrow \cdot OH \quad (7)$$

$$O_2^{\cdot -} + H^+ \rightarrow HO_2^{\cdot} \quad (8)$$

$$2HO_2^{\cdot} \rightarrow H_2O_2 + O_2 \quad (9)$$

$$H_2O_2 + e^-_{cb} \rightarrow \cdot OH + OH^- \quad (10)$$

$$C_6H_5ClO + \cdot OH \rightarrow \text{intermediates} \rightarrow CO_2 + H_2O + Cl^- \quad (11)$$

Thus, when the dopant content is relatively high, the metal ions are converted into recombination points for positive holes because they are negatively charged by the electrons, thereby decreasing the photocatalytic activity.

Fig. 11 shows the effect of the doping amount on the initial removal rate and degradation percentage of 4CP. It can be seen that the best results are obtained at low amounts of dopant as above mentioned. Samples DW1 and DM1 exhibited similar initial rates of approximately 46.8×10^{-8} mol/g_{cat} seg, but sample DM1 obtained 7% higher degradation than DW1 sample.

With the purpose of evaluating the deep oxidation of 4-chlorophenol by photocatalyst, carbon organic total (TOC) was determined at the end of the reaction for all photocatalysts as shown in Fig. 12. The mineralization of the parent compound was observed according to the following general route [40,41]:

$$4CP + TiO_2 + hv \rightarrow \text{Intermediates} \rightarrow CO_2 + H_2O + Cl^- \quad (12)$$

The TOC reduction of 4CP was 69% when DW1 photocatalyst is used. Sample DM1 showed 65% reduction of TOC while prepared pure TiO_2 and Degussa P25 exhibited 44% and 34%, respectively. This shows that the photo-oxidation of TiO_2 doped with low weight percentages of W or Mo ions was not only degradation but also mineralization of organic molecules occurs. Reduction profiles of TOC as a function of time irradiation for these photocatalysts are shown in Fig. 13. In addition, the initial mineralization rates were estimated and they are presented in Table 3. Although DW1 sample exhibited less degradation than DM1 sample, this showed the highest mineralization with an initial mineralization rate of 21.82×10^{-3} mg/g_{cat} s. This may be because DW1 contains lower atomic percentage of tungsten in TiO_2 matrix which leads to efficient charge separation and consequently better photoactivity. It is noteworthy that pure synthesized titania presented better degradation and mineralization of 4CP compared with Degussa P25 due to its high surface area, low crystallinity, mesoporous

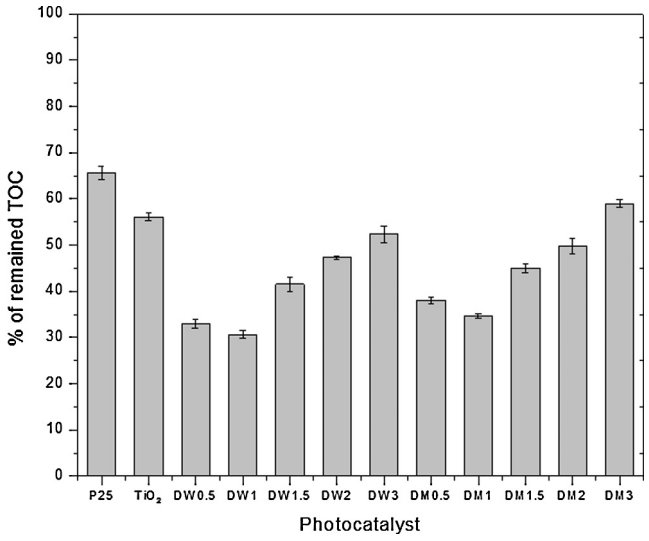

Fig. 12. Effect of the type of photocatalyst on % of remained TOC after 100 min of reaction.

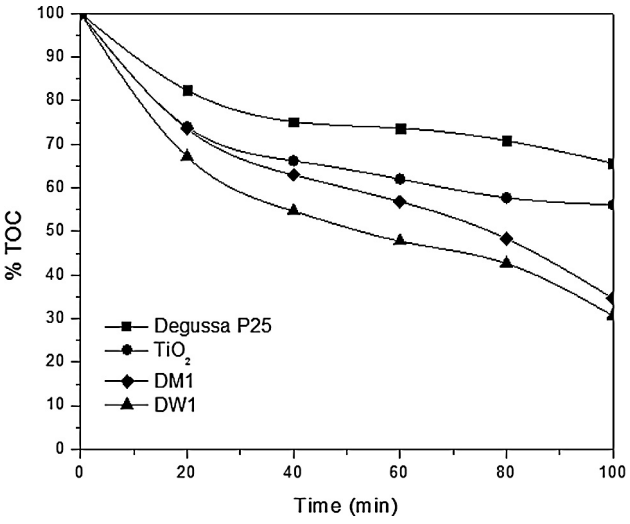

Fig. 13. Reduction profiles of total organic carbon content (TOC) during the photocatalytic activity.

structure, and only presence of anatase crystalline structure [42], but the absence of electron acceptor species generated the lowest photocatalytic activities in both materials.

Since for both dopants, W and Mo, the highest photocatalytic activity was found to be with 1%, it was decided to test catalysts with 0.5 wt.% and 1.5 wt.%. The obtained results are also shown in Figs. 9, 11 and 12. It can be observed that albeit the catalyst doped with 0.5% W exhibits the highest initial reaction rate, after the assessed reaction time the 4CP conversion is lower than with the 1% W doped titania and therefore it can be considered the most active towards 4CP degradation. In the case of Mo cations, the initial reaction rate is lower with 0.5 wt.% than with 1 wt.%. This suggests that at lower wt.% than 1 the photogenerated charges are not as efficiently trapped and this might be due to the amount of dopant cations being insufficient to reduce h^+/e^- pairs recombination. Then, it can be concluded that the improvement in 4CP degradation/mineralization increases with increasing doping up to 1% and then decreases when dopant content exceeds this value. This in concordance with related literature [43].

Table 3
Initial mineralization rates and mineralization percentages of 4CP.

Sample ID	4CP mineralization rate $\times 10^3$ (mg/g_{cat} seg)	4CP mineralization (%)
DW1	21.82	69
DM1	18.28	65
TiO_2	19.43	44
Degussa P25	12.19	34

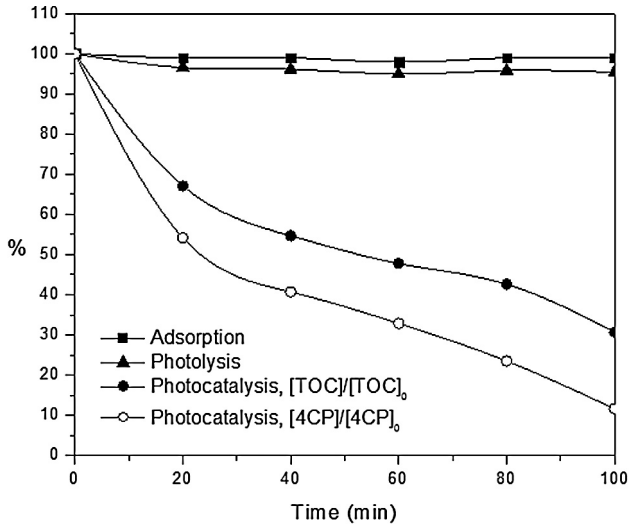

Fig. 14. Effect of adsorption, photolysis and photocatalysis on the degradation and mineralization of 4CP over W-doped TiO_2 1.0 wt.% (sample DW1).

Fig. 14 shows the effect of photolysis and adsorption with the sample that showed the highest photocatalytic activity in terms of the lowest remaining amount of TOC at 100 min. The photolysis was performed by irradiating the 4CP solution in the absence of catalyst and the adsorption was carried out with photocatalyst in darkness. Additionally, no effect was observed on the removal of 4CP by both, adsorption nor photolysis.

As can be seen in Fig. 14, the complete reduction of initial TOC content was not achieved and this implies an incomplete mineralization of organic compound. 4-chlorocatechol, benzoquinone and hydroquinone have been identified and quantified as the main intermediate compounds formed during photocatalytic degradation of 4-chlorophenol [22,44], which can be identified by GC–MS, HPLC or LC-MS techniques. Although this characterization is quite interesting, it is not part of the main objective of this work.

4. Conclusions

Titania doped with tungsten and molybdenum cations by EISA method were successfully prepared. Their photocatalytic activity was studied on the degradation and mineralization of 4-chlorophenol as organic pollutant. All doped materials exhibited higher degradation than Degussa P25 and pure titania due to the presence of cations into anatase TiO_2 lattice and without requiring oxygen supply. Electrons are trapped more effectively on low amounts of W^{6+} and Mo^{6+} ions decreasing the recombination rate, but also larger amounts of hydroxyl radicals are generated in the holes through which the oxidation processes are conducted. W–doped TiO_2 with 1 wt.% was found to provide the highest activity for the mineralization of 4CP with 69% reduction of initial TOC compared to Degussa P25 and pure TiO_2 that reduced 34% and 44%, respectively.

Acknowledgements

Authors are grateful to PRODEP – Mexico and CONACYT – Mexico for financial support through projects 103.5/13/5257 and 168305, respectively. Osmín Avilés-García thanks CONACYT – Mexico for scholarship 378292 and CCIQS UAEM-UNAM for the granted support. The technical support of Uvaldo Hernandez Balderas, Rafael Vilchis Nestor, Gustavo Lopez Tellez and L.I.A. María Citlalit Martínez Soto is also acknowledged.

Appendix A. Supplementary data

Supplementary data associated with this article can be found, in the online version, at http://dx.doi.org/10.1016/j.fuel.2016.10.005.

References

[1] Herrmann J-M. Catal Today 1999;53:115–29.
[2] Daneshvar N, Rabbani M, Modirshahla N, Behnajady MA. J Photochem Photobiol A: Chem 2004;168:39–45.
[3] Padmini E, Miranda LR. Chem Eng J 2013;232:249–58.
[4] M.A Carreon, V.V. Guliants, Amsterdam: Elsevier; 2009 p. 413–39.
[5] Soler-Illia GJdAA, Louis A, Sanchez C. Chem Mater 2002;14:750–9.
[6] Janda V, Svecova M. Chem List 2000;94:905–8.
[7] Al-Ekabi H, Serpone N. J Phys Chem 1988;92:5726–31.
[8] Shamaila S, Sajjad AKL, Chen F, Zhang J. Mater Res Bull 2010;45:1375–82.
[9] Wongwisate P, Chavadej S, Gulari E, Sreethawong T, Rangsunvigit P. Desalination 2011;272:154–63.
[10] Blanco M, Pizzio L. Appl Catal A: Gen 2011;405:69–78.
[11] Al-Ekabi H, Serpone N, Pelizzetti E, Minero C, Fox MA, Draper RB. Langmuir 1989;5:250–5.
[12] Yamazaki S, Fujiwara Y, Yabuno S, Adachi K, Honda K. Appl Catal B: Environ 2012;121–122:148–53.
[13] Devi GS, Hyodo T, Shimizu Y, Egashira M. Sensors Actuator B Chem 2002;87:122–9.
[14] Pullar RC, Penn SJ, Wang X, Reaney IM, Alford NM. J Eur Ceram Soc 2009;29:419–24.
[15] Devi S, Jha AK. Phys B Cond Matt 2009;404:4290–4.
[16] Gomathi Devi L, Narasimha Murthy B. Catal Lett 2008;125:320–30.
[17] Wang E, Yang W, Cao Y. J Phys Chem C 2009;113:20912–7.
[18] Devi LG, Murthy BN, Kumar SG. J Mol Catal A: Chem 2009;308:174–81.
[19] Lorret O, Francová D, Waldner G, Stelzer N. Appl Catal B: Environ 2009;91:39–46.
[20] Peng T, Song H, Xiao J, Liu H, Qin J. J Non-Cryst Sol 2006;352:3167–74.
[21] Pozan GS, Kambur A. Appl Catal B: Environ 2013;129:409–15.
[22] Silva AMT, Silva CG, Dražić G, Faria JL. Catal Today 2009;144:13–8.
[23] Ohno T, Sarukawa K, Tokieda K, Matsumura M. J Catal 2001;203:82–6.
[24] Zhu J, Chen F, Zhang J, Chen H, Anpo M. J Photochem Photobiol A: Chem 2006;180:196–204.
[25] Grabowska E, Sobczak JW, Gazda M, Zaleska A. Appl Catal B: Environ 2012;117–118:351–9.
[26] Cheng X, Yu X, Xing Z. J Colloid Interface Sci 2012;372:1–5.
[27] Jeon MS, Yoon WS, Joo H, Lee TK, Lee H. Appl Surf Sci 2000;165:209–16.
[28] Zhou M, Yu J, Cheng B, Yu H. Mater Chem Phys 2005;93:159–63.
[29] Yeung KL, Yau ST, Maira AJ, Coronado JM, Soria J, Yue PL. J Catal 2003;219:107–16.
[30] Christy AA, Kvalheim OM, Velapoldi RA. Vib Spectrosc 1995;9:19–27.
[31] Gassim FA-ZG, Alkhateeb AN, Hussein FH. Desalination 2007;209:342–9.
[32] Gutiérrez-Alejandre A, Ramírez J, Busca G. Catal Lett 1998;56:29–33.
[33] Kubacka A, Colón G, Fernández-García M. Appl Catal B: Environ 2010;95:238–44.
[34] Yang Y, Li X-J, Chen J-T, Wang L-Y. J Photochem Photobiol A: Chem 2004;163:517–22.
[35] Kubacka A, Colón G, Fernández-García M. Catal Today 2009;143:286–92.
[36] Huang DG, Liao SJ, Zhou WB, Quan SQ, Liu L, He ZJ, Wan JB. J Phys Chem Solids 2009;70:853–9.
[37] Cheng X, Yu X, Li B, Yan L, Xing Z, Li J. Mater Sci Eng B 2013;178:425–30.
[38] Venkatachalam N, Palanichamy M, Arabindoo B, Murugesan V. J Mol Catal A: Chem 2007;266:158–65.
[39] Galindo C, Jacques P, Kalt A. J Photochem Photobiol A: Chem 2000;130:35–47.
[40] Sharma S, Mukhopadhyay M, Murthy ZVP. J Ind Eng Chem 2012;18:249–54.
[41] Li X, Cubbage JW, Tetzlaff TA, Jenks WS. J Org Chem 1999;64:8509–24.
[42] Sakatani Y, Grosso D, Nicole L, Boissiere C, Soler-Illia GJdeAA, Sanchez C. J Mater Chem 2006;16:77–82.
[43] Yu F, Wang Y, Tang H, Zhang Y, Jin C, Liu X, Li M, Wang J. Catal Commun 2014;51:46–52.
[44] Elghniji K, Hentati O, Mlaik N, Mahfoudh A, Ksibi M. J Environ Sci 2012;24:479–87.